The detection of benzene in Saturn's upper atmosphere

AGU PUBLICATIONS

Geophysical Research Letters

RESEARCH LETTER
10.1002/2016GL070000

Key Points:
- We present the first detections of benzene and hydrocarbon haze in their production region in Saturn's upper atmosphere
- The observed benzene abundances can be explained by solar-driven ion chemistry that is enhanced at high latitudes in the north

Supporting Information:
- Supporting Information S1

Correspondence to:
T. T. Koskinen,
tommi@lpl.arizona.edu

Citation:
Koskinen, T. T., J. I. Moses, R. A. West, S. Guerlet, and A. Jouchoux (2016), The detection of benzene in Saturn's upper atmosphere, *Geophys. Res. Lett.*, *43*, 7895–7901, doi:10.1002/2016GL070000.

Received 10 JUN 2016
Accepted 1 AUG 2016
Accepted article online 4 AUG 2016
Published online 15 AUG 2016

The detection of benzene in Saturn's upper atmosphere

T. T. Koskinen[1], J. I. Moses[2], R. A. West[3], S. Guerlet[4], and A. Jouchoux[5]

[1]Lunar and Planetary Laboratory, University of Arizona, Tucson, Arizona, USA, [2]Space Science Institute, Boulder, Colorado, USA, [3]Jet Propulsion Laboratory, California Institute of Technology, Pasadena, California, USA, [4]Laboratoire de Météorologie Dynamique/IPSL, CNRS, UPMC University of Paris 06, Sorbonne Universités, Paris, France, [5]Laboratory for Atmospheric and Space Physics, University of Colorado Boulder, Boulder, Colorado, USA

Abstract The stratosphere of Saturn contains a photochemical haze that appears thicker at the poles and may originate from chemistry driven by the aurora. Models suggest that the formation of hydrocarbon haze is initiated at high altitudes by the production of benzene, which is followed by the formation of heavier ring polycyclic aromatic hydrocarbons. Until now there have been no observations of hydrocarbons or photochemical haze in the production region to constrain these models. We report the first vertical profiles of benzene and constraints on haze opacity in the upper atmosphere of Saturn retrieved from Cassini Ultraviolet Imaging Spectrograph stellar occultations. We detect benzene at several different latitudes and find that the observed abundances of benzene can be produced by solar-driven ion chemistry that is enhanced at high latitudes in the northern hemisphere during spring. We also detect evidence for condensation and haze at high southern latitudes in the polar night.

1. Introduction

Dissociation of methane by solar UV photons and precipitating electrons in the upper atmospheres of the giant planets is believed to initiate complex chemistry that produces cyclic benzene (C_6H_6) as a first step toward the synthesis of heavier polycyclic aromatic hydrocarbons (PAHs) and stratospheric haze [*Friedson et al.*, 2002; *Wong et al.*, 2000, 2003]. Previous observations of benzene are limited to column-integrated abundances derived from a few infrared emission measurements of Jupiter and Saturn in the ν_4 band (14.84 μm) that probe the stratosphere (~1 mbar) well below the photochemical production peak (~0.1–1 μbar). On Jupiter, these emissions are brighter in the auroral region than on the disk [*Kim et al.*, 1985; *Bézard et al.*, 2001] and the same appears to be true on Saturn where Cassini/ Composite Infrared Spectrometer (CIRS) has achieved a 2–3σ detection near the southern auroral oval [*Guerlet et al.*, 2015]. Theoretical models for Jupiter predict that particle precipitation in the aurora and subsequent ion chemistry produces peak benzene abundances of a few times 10^{-8} in the upper atmosphere [*Wong et al.*, 2003]. Current observations of the giant planets allow for peak abundances ranging from 10^{-10} to 10^{-6} [*Bézard et al.*, 2001]. More precise constraints on the models are clearly required.

The Cassini/UVIS instrument has observed more than 40 stellar occultations by Saturn between 2005 and 2015. These observations probe the upper atmosphere at different latitudes, including absorption at wavelengths from 560 to 1910 Å in the EUV and FUV channels [*Esposito et al.*, 2004]. To date, the occultations have been used to retrieve the temperature and density structure of the thermosphere, while densities for CH_4, C_2H_2, C_2H_4, and C_2H_6 in the upper stratosphere and mesosphere have also been retrieved from a few occultations [*Shemansky and Liu*, 2012; *Koskinen et al.*, 2013, 2015]. Here we analyze new occultations and report the first detection of benzene in the UVIS data that uniquely probe the photochemical production region. We also present evidence for a high-altitude FUV continuum absorber that resembles aerosol extinction on Titan [*Liang et al.*, 2007; *Koskinen et al.*, 2011] in one of the new occultations.

2. Methods

We detect pronounced absorption by benzene in three Cassini/UVIS stellar occultations that probe planetographic latitudes of 48.9°S in April 2005, 74.3°N in September 2012, and 72.7°S in January 2015 (occultations ST05M04D13S49, ST12M09D04N74, and ST15M01D08S73, respectively) and weaker but statistically significant absorption at other locations (see Table 1). In addition, we detect absorption by CH_4, C_2H_2, C_2H_4,

Table 1. Cassini/UVIS Occultations

ID	Date[b]	Target	ϕ_{pg} (deg)	LST[a]	L_s (deg)
ST05M04D13S49	04/13/2005	δ Ori	48.9°S	15:46	303.5
ST08M12D16N2	12/16/2008	α Cru	1.8°N	18:57	351.8
ST08M12D16N22	12/16/2008	β Cen	21.7°N	01:13	351.8
ST09M01D03S5	1/3/2009	β Cru	4.6°S	18:27	352.4
ST09M01D22S5	1/22/2009	β Cru	4.5°S	18:26	353.1
ST10M07D05S6	7/5/2010	α Vir	6.3°S	07:10	11.1
ST12M09D04N74	9/4/2012	β CMa	74.3°N	14:36	36.9
ST14M10D03S8	10/3/2014	ζ Pup	7.6°S	09:46	60.7
ST15M01D08S73	1/8/2015	α Vir	72.7°S	10:02	63.7
ST15M02D18N2	2/18/2015	κ Ori	2.1°N	19:54	65.0
ST15M10D01N28	10/1/2015	ζ Ori	28.1°N	19:26	71.8
ST15M10D01N40	10/1/2015	ϵ Ori	39.9°N	19:28	71.8
ST15M10D01N57	10/1/2015	δ Ori	57.1°N	19:40	71.8
ST15M10D01N35	10/1/2015	ζ Ori	34.8°N	07:13	71.8
ST15M10D15N29	10/15/2015	ζ Ori	28.8°N	19:25	72.2
ST15M10D15N41	10/15/2015	ϵ Ori	40.6°N	19:27	72.2
ST15M10D15N58	10/15/2015	δ Ori	57.9°N	19:39	72.2
ST15M10D29N36	10/29/2015	ζ Ori	35.6°N	07:09	72.7

[a]Planetographic latitude (ϕ_{pg}) and local solar time (LST) on a "24 h clock" apply to the half-light point of the 1550–1600 Å light curves in the FUV channel. The occultation ID is constructed from the label ST followed by year, month (M), day (D), and south (S) or north (N) rounded latitude.
[b]Dates are formatted as month/day/year.

and C_2H_6 in all of the occultations (see section 3.1). We fit column densities to the observed line of sight (LOS) transmission spectra at each tangent altitude by using the Levenberg-Marquardt (L-M) method [*Press et al.*, 1992]. We then invert the resulting column density profiles by using Tikhonov regularization to obtain number densities [*Koskinen et al.*, 2011, 2015]. More details on the data reduction and analysis are provided in the supporting information.

In order to derive hydrocarbon volume mixing ratios from the retrieved density profiles for the occultations, we build atmospheric structure models based on temperature-pressure (T-P) profiles retrieved from the occultations for the thermosphere and Cassini/CIRS observations for the stratosphere. We focus on the three occultations identified above because they provide the clearest detections of C_6H_6. For ST05M04D13S49, we use a CIRS limb scan at 45°S from 25 February 2006 [*Guerlet et al.*, 2009]. For ST12M09D04N74, we use T-P profiles fitted to the CIRS nadir observations around the north pole interpolated to the latitude and time of the UVIS occultation [*Fletcher et al.*, 2015]. For ST15M01D08S73, we retrieve a new T-P profile by obtaining a simultaneous best fit to the UVIS occultation and CIRS limb observations at 77°S from 16 June 2015. Our atmosphere structure models are also designed to fit the H_2 and CH_4 densities as a function of altitude from UVIS that constrain the temperature connection between CIRS and UVIS [*Koskinen et al.*, 2015]. More details on the atmosphere models here are provided in the supporting information.

3. Results

3.1. Detection of Benzene

The detection of benzene in the UVIS data is illustrated by Figure 1, which shows the average line of sight (LOS) optical depth at tangent altitudes of 440–475 km above the 1 bar level for ST15M01D08S73, a high-signal to noise (S/N) occultation of α Virginis. Figure S1 in the supporting information shows a similar plot for ST12M09D04N74. Absorption by C_2H_2 and C_2H_4 is clearly present at 1430–1900 Å while absorption by CH_4 and C_2H_6 is also detected at shorter wavelengths (not shown). As we state above, we fit column densities to the LOS spectra by using the L-M method. The red lines in Figure 1 show the best fits that exclude benzene.

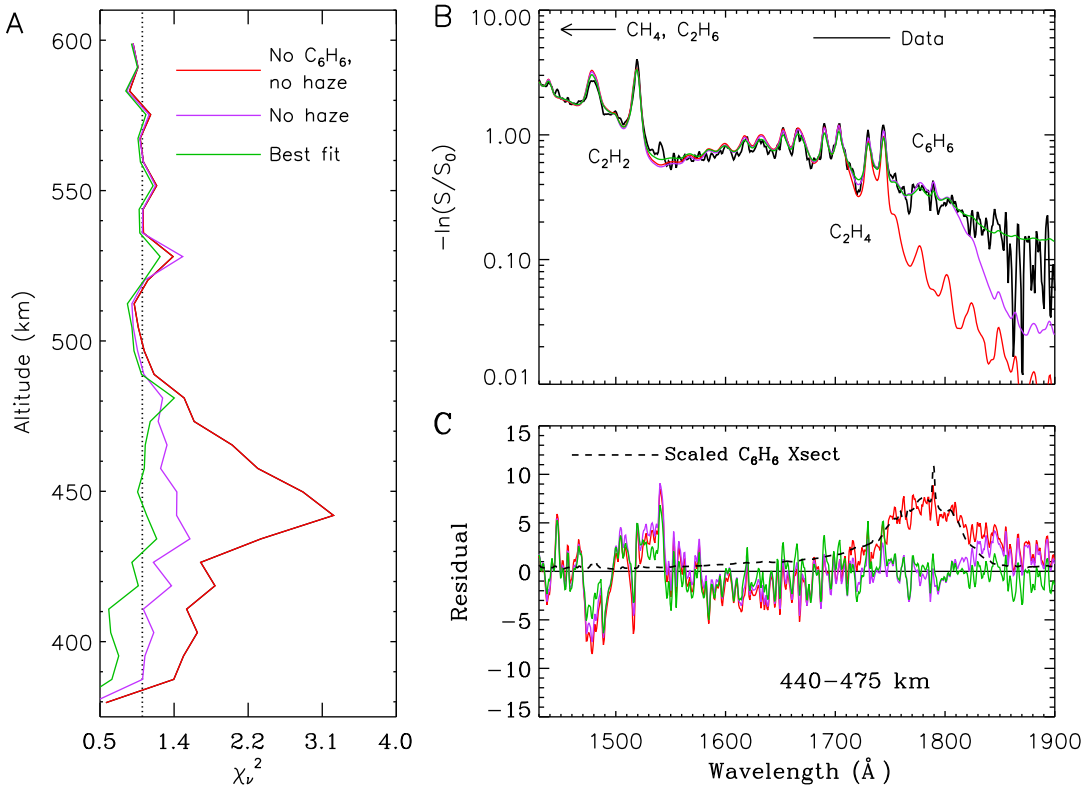

Figure 1. Detection of benzene and continuum (haze) absorption in occultation ST15M01D08S73 at a planetographic latitude of 72.7°S from January 2015 (Table 1). (a) χ_ν^2 for our best fits to the data at different tangent altitudes together with fits that exclude benzene and haze. (b) Average optical depth at tangent altitudes of 440–475 km above the 1 bar level (average of five spectra) with the same model fits. (c) Residual for the model fits at 440–475 km. The residual is defined as $(\tau_d - \tau_m)/\sigma$ where τ_d is the observed optical depth, τ_m is the model optical depth, and σ is the measurement error. The dashed line shows the scaled absorption cross section of benzene from *Capalbo et al.* [2016]. The cross section is shown for illustration purposes and has not been properly convolved by the UVIS line spread function that is included in the forward model.

The residual includes missing absorption at 5–10σ level that matches absorption by benzene. The best fits with benzene (purple lines) are clearly better, reducing χ_ν^2 significantly below 480 km. The observed spectrum also includes a small peak around 1789 Å that is reproduced by our best fit forward model and coincides with the second Rydberg transition of benzene in the $^1A_{1g}-{}^1E_{1u}$ valence π-electron band [*Capalbo et al.*, 2016].

The signature of benzene in Figures 1, S1, and S7 is essentially the same that was used to detect benzene in UVIS stellar occultations by Titan [*Koskinen et al.*, 2011; *Capalbo et al.*, 2016]. The inclusion of benzene in the forward models in Figures 1 and S1 leads to a statistically good fit to the data at all relevant tangent altitudes and, as we show below, the abundances that we retrieve concur with ion chemistry models for Saturn and Jupiter (see sections 3.2 and 3.3). We have also created a synthetic occultation to further support the identification of the absorbers in the data and demonstrate that our retrieval method can be used to reliably retrieve their densities from the spectra. The details of this exercise, together with a more detailed discussion of the fit residuals, are provided in the supporting information.

3.2. Distribution of Benzene

Our retrieval yields hydrocarbon number densities as a function of radial distance from Saturn's center (see Figure S4) that we convert to volume mixing ratios as a function of pressure by using the atmosphere structure models described in section 2. The resulting peak mixing ratios of benzene at 0.1–10 μbar range from about 2×10^{-8} for ST15M01D08S73 to 5×10^{-7} for ST12M09D04N74 (see Figure 2). The uncertainties in the observed hydrocarbon mixing ratios in Figure 2 are based on the uncertainties in their retrieved number densities and do not include the uncertainty in the atmosphere model density. In regions of overlap for the retrieved species, the C_6H_6/CH_4 density ratio provides a more robust measure of the abundance of benzene because it does not depend on the full atmosphere model. We find maximum C_6H_6/CH_4 density ratios of 4.7×10^{-5} at 72.7°S and 10^{-3} at 74.3°N. These abundances are much larger than predictions based on

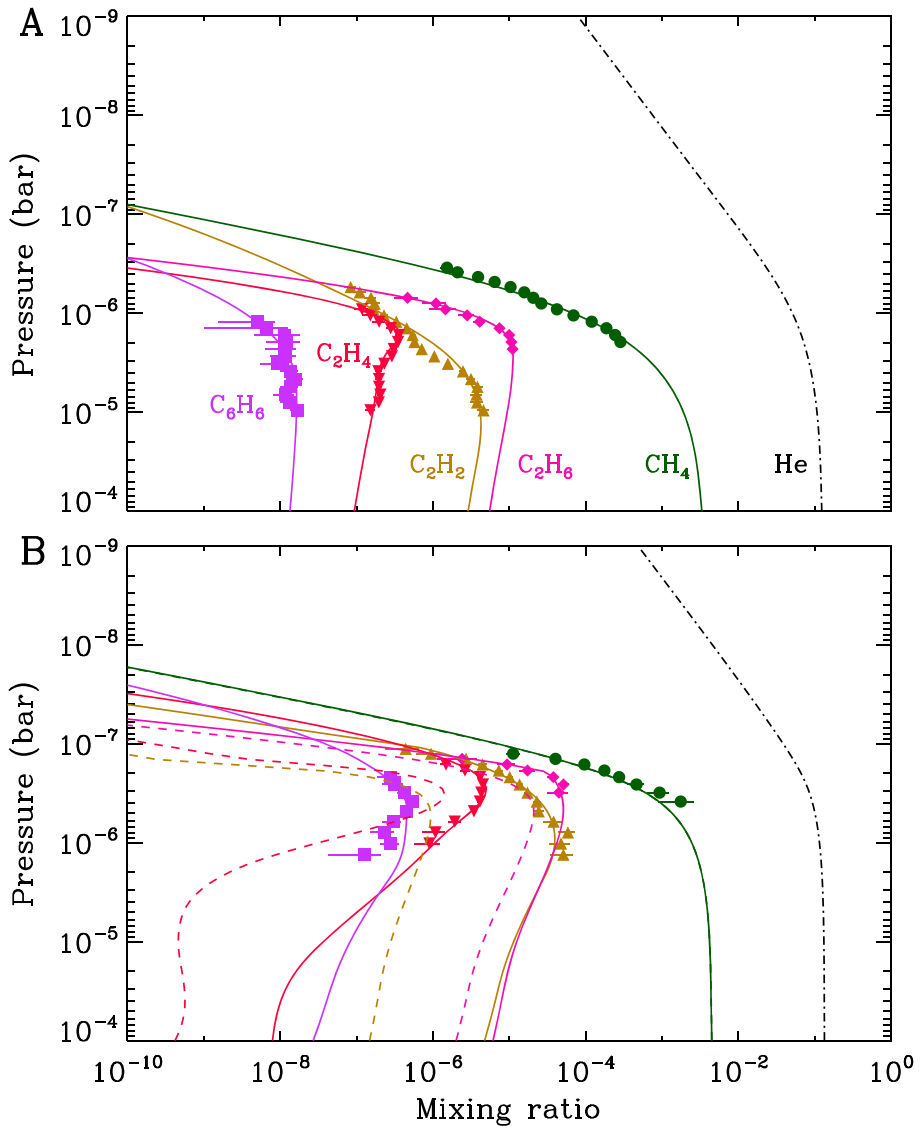

Figure 2. Hydrocarbon volume mixing ratios derived from the Cassini/UVIS occultations (symbols) and photochemical model results (lines). (a) Planetographic latitude 72.7°S, January 2015 (ST15M01D08S73). (b) Planetographic latitude 74.3°N, September 2012 (ST12M09D04N74) (see Table 1). Solid lines show models that include extra production to match the observations, and dashed lines show results based on solar-driven neutral photochemistry. Note that the occultation at 72.7°S probed the polar night and all production is extra production. The mixing ratio of C_6H_6 based on solar-driven neutral photochemistry for ST12M09D04N74 is less than 10^{-10} and not shown here.

solar UV-driven neutral photochemistry that produces a peak benzene mixing ratio of 2×10^{-10} at 0.4 mbar [*Moses and Greathouse*, 2005].

We note that the CIRS limb and UVIS observations are separated in time by at most 5 months. Accounting for seasonal change and the possibility of short-term wave activity, the variability in stratospheric temperatures is up to 5 K above the 10 mbar level [e.g., *Sylvestre et al.*, 2015]. This translates to an uncertainty of about 15 km in the pressure level altitudes at 1 μbar and thus a factor of ~1.3 in the atmosphere model density. Allowing for a larger uncertainty of 10 K above the 10 mbar level in the atmosphere model for ST12M09D04N74 that relies on CIRS nadir data translates to a factor of ~1.7 in the model density at 1 μbar.

We also detect evidence for benzene at other latitudes. Figure 3 shows the maximum C_6H_6/CH_4 density ratio as a function of latitude based on our observations. The ratio increases with latitude in the northern hemisphere during spring. It is also more than an order of magnitude lower at high southern latitudes for ST15M01D08S73 than at similarly high northern latitudes for ST12M09D04N74. Previous work suggests that the production of

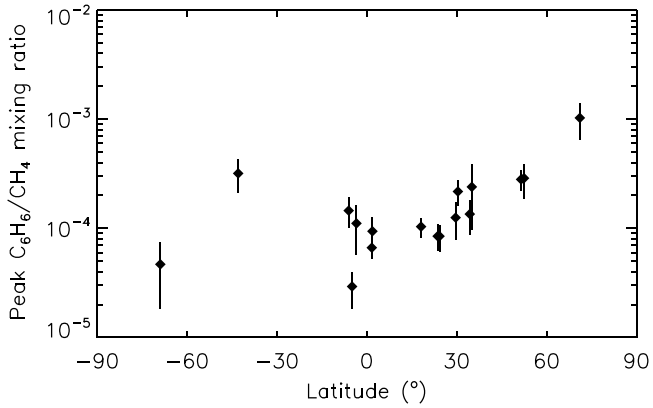

Figure 3. Maximum C_6H_6/CH_4 density ratio at 0.1–10 μbar as a function of latitude.

benzene is mostly driven by electron precipitation in the aurora. If this is the case, the detection of benzene at lower latitudes and near the equator implies that efficient meridional transport from high latitudes is possible despite the Coriolis barrier imposed by Saturn's fast rotation. The alternative is that solar-driven ion chemistry plays a significant role in the production of benzene.

3.3. Production of Benzene and High-Latitude Atmosphere

As we note above, benzene has also been detected in UVIS occultations by Titan, with a peak volume mixing ratio of about 10^{-5}–10^{-4} in the upper atmosphere [*Capalbo et al.*, 2016]. Photochemical models for Titan show that benzene is primarily produced by ion chemistry through the electron recombination of $C_6H_7^+ + e \rightarrow C_6H_6 + H$ [*Vuitton et al.*, 2008]. The same reaction is also likely to dominate high-altitude production of benzene on the giant planets [*Wong et al.*, 2003], but there are currently no published models that include $C_6H_7^+$ or the production of benzene by ion chemistry on Saturn. The theoretical investigation that comes closest to doing so is from *Kim et al.* [2014] who modeled hydrocarbon ion chemistry on Saturn. These authors, however, did not track individual ions with more than four carbon atoms. Instead, they considered the chemistry of a generic group $C_6H_n^+$ ion while keeping the neutral densities fixed in their model. Adapting full ion chemistry to Saturn is beyond the scope of this paper. Instead, we use the neutral photochemistry model of *Moses et al.* [2015] to infer the extra production rate that is required to explain the observed abundance of benzene.

The ST05M04D13S49 occultation probed the midlatitude summer hemisphere at 48.9°S planetographic latitude (L_s =303.5°). We require a peak production rate of 1.2×10^6 m^{-3} s^{-1} at 0.3 μbar to match the observed abundance of benzene at this location (see supporting information and Figure S6). The neutral chemistry production rate of 2 m^{-3} s^{-1} at the same pressure level is much lower than the required production rate. However, the required production rate is roughly consistent with the production rate expected from electron recombination of $C_6H_7^+$ if about half of the $C_6H_n^+$ ions in the solar-driven model of *Kim et al.* [2014] are from $C_6H_7^+$. This is reasonable because roughly half of the $C_6H_n^+$ ions measured by the Ion Neutral Mass Spectrometer on Titan were from $C_6H_7^+$ [e.g., *Cui et al.*, 2009]. Therefore, solar-driven ion chemistry alone may be sufficient to explain the observed abundance of benzene for ST05M04D13S49. We also find that the neutral photochemical models need an extra production source of the other hydrocarbons in order to fit the UVIS occultation data, particularly the unsaturated hydrocarbons C_2H_2 and C_2H_4. More details on the model and fitting the abundances of the other hydrocarbons are provided in the supporting information.

The ST12M09D04N74 occultation probed the northern spring hemisphere at 74.3°N planetographic latitude (L_s=36.9°). At the time of the occultation in 2012, this location received a similar daily mean actinic flux as ST05M04D13S49, which probed summer midlatitudes. The column-integrated production rate of benzene that we retrieve in the upper atmosphere for this case is 5 times higher than the required rate for ST05M04D13S49. Given that the C_6H_6/CH_4 abundance ratio also increases with latitude in the northern hemisphere, the inferred production rates support the idea that the aurora enhance the production rates of benzene and other hydrocarbons at high northern latitudes. The ST15M01D08S73 occultation probed a similar location to ST12M09D04N74 in the southern hemisphere, at 72.7°S planetographic latitude (L_s = 63.7°). This location, however, entered the polar night a year prior to the occultation and it also lies 3–6° latitude equatorward from the main auroral oval. The lifetimes of the photochemical products are sufficient so that they can be transported to this location either from the sunlit atmosphere or the aurora. The hydrocarbon abundances, however, are significantly lower than the high-latitude abundances in the northern spring hemisphere.

Our models for ST12M09D04N74 and ST15M01D08S73 are the first complete atmosphere structure models for high latitudes on Saturn derived from observations. These models are useful for the interpretation of airglow

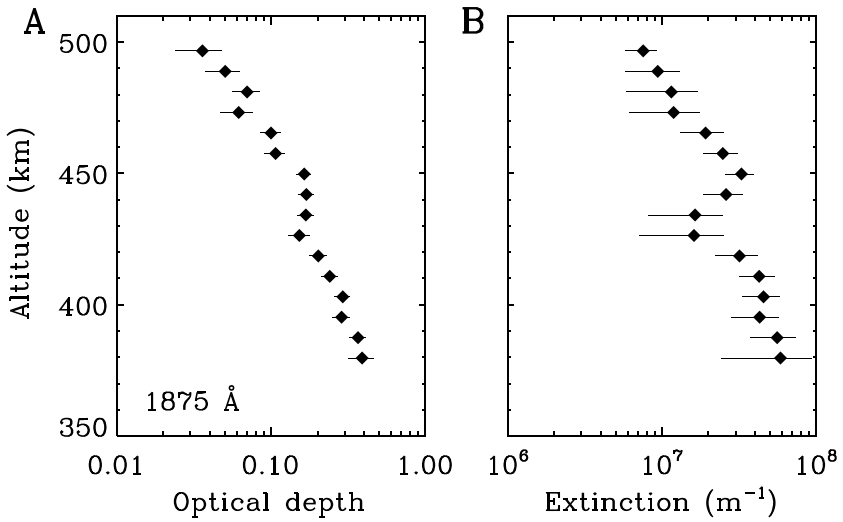

Figure 4. Optical depth and extinction at 1875 Å derived for the UV continuum absorber (aerosols) at the planetographic latitude 72.7°S in January 2015 (ST15M01D08S73, Table 1). (a) Optical depth. (b) Extinction.

and auroral emissions. In both cases, the base of the thermosphere near ~1 μbar is substantially deeper than at lower latitudes (see Figure S5 and the results in *Koskinen et al.* [2015]). For ST15M01D08S73, a deep thermosphere is also required to match the CIRS thermal infrared emissions from CH_4 in limb geometry. In addition, the CH_4 profiles in Figure 2 indicate that the homopause for ST15M01D08S73 is deeper than that for ST12M09D04N74. We find that the most likely explanation for the difference in the CH_4 profiles between ST12M09D04N74 and ST15M01D08S73 is a relative downwelling of about −1 cm s^{-1} that reduces the abundance of CH_4 at low pressures for ST15M01D08S73 (see supporting information for further details). Such a wind can be part of a seasonal circulation pattern in the winter hemisphere or alternating regions of upwelling and downwelling that vary with longitude near the aurora [*Müller-Wodarg et al.*, 2012].

3.4. High-Altitude Haze

We detect evidence for haze in the ST15M01D08S73 data at tangent altitudes below 470 km (see Figure 1), with absorption extending to the 1800–1900 Å wavelength window where hydrocarbon absorption is weak. This is the only occultation in which we firmly detect this continuum absorption, which is similar to extinction by haze on Titan [*Liang et al.*, 2007; *Koskinen et al.*, 2011]. The CIRS data also include a strong aerosol signature in the stratosphere near this location. In the absence of detailed information about the properties of high-altitude hazes on Saturn, we fit the UVIS data by using the optical properties of spherical tholins that are often adopted to simulate Titan aerosols [e.g., *Koskinen et al.*, 2011]. Effectively, this sets the wavelength dependency of the slant optical depth due to haze, which is often written as

$$\tau_\lambda \sim \tau_0 \left(\lambda_0/\lambda\right)^\alpha \quad (1)$$

where τ_0 is a reference value at wavelength λ_0, while α depends on the particle type. We find that $\alpha = 2-3$ provide the best fit to the data (see Figure S7 and supporting information for further details). We do not advocate that the high-altitude haze actually consists of tholins. The exact identity of the continuum absorber remains a mystery and, as on Titan, it may consist of a combination of higher-order hydrocarbons. This conclusion agrees with *Kim et al.* [2012] who interpreted absorption at 3–4 μm detected by Cassini Visual and Infrared Mapping Spectrometer (VIMS) as absorption by Saturnian haze composed of such hydrocarbons.

The slant optical depth of the haze at 1875 Å increases from 0.1 at 450 km (3.2 μbar) to 0.4 at 380 km (16 μbar) (see Figure 4). The corresponding extinction coefficient increases from 10^{-8} m^{-1} around 470 km to 10^{-7} m^{-1} around 380 km. The fact that we do not see the signature of the haze in other occultations is intriguing, particularly because ST15M01D08S73 probes the polar night. This may be because the deep homopause allows us to probe higher pressures than, say, at high northern latitudes with ST12M09D04N74 (see Figure 2). With a temperature of 125 K, the mesosphere for ST15M01D08S73 is also remarkably cold (see Figure S5). As a result, the saturation mixing ratio for C_6H_6 [*Fray and Schmitt*, 2009] decreases to less than 10^{-7}–10^{-6} below the 1 μbar level for ST15M01D08S73. This is in contrast to ST05M04D13S49 or ST12M09D04N74 where the

saturation mixing ratio is 10^{-4}–10^{-3} near the 1 μbar level. Thus, the cold mesosphere in the polar night can promote condensation of benzene and heavier hydrocarbons to form haze.

4. Conclusions

We present new results based on Cassini/UVIS stellar occultations and photochemical models that address the formation of benzene and hazes on Saturn. We find benzene at multiple latitudes with abundances that cannot be explained by solar-driven neutral photochemistry but can be produced by solar-driven ion chemistry enhanced by auroral production at high latitudes. The detected abundances are, in principle, sufficient for the production of PAHs and stratospheric hazes even at low to middle latitudes. However, we only detect firm evidence for the presence of haze in one of the UVIS occultations that probes high southern latitudes in the polar night where cold mesospheric temperatures can lead to condensation of benzene and heavier hydrocarbons. Our results provide the first atmosphere structure models for the high-latitude upper atmosphere and motivation for detailed studies of ion chemistry and photochemical hazes in Saturn's upper atmosphere.

Acknowledgments
T.T.K. was supported by the NASA Cassini Data Analysis and Participating Scientist grant NNX14AD51G. J.I.M. gratefully acknowledges support from NASA Solar System Workings grant NNX16AG10G. Part of this work was performed by the Jet Propulsion Laboratory, California Institute of Technology, with funding from the Cassini Project for R.A.W. S.G. was supported by CNES. This work is based on observations with the UVIS and CIRS instruments onboard Cassini. The retrieval results and atmosphere models discussed in this work can be obtained from the authors by emailing T.T.K.

References

Bézard, B., P. Drossart, T. Encrenaz, and H. Feuchtgruber (2001), Benzene on the giant planets, *Icarus*, *154*, 492–500.
Capalbo, F. J., et al. (2016), New benzene absorption cross sections in the VUV, relevance to Titan's upper atmosphere, *Icarus*, *265*, 95–109.
Cui, J., et al. (2009), Analysis of Titan's neutral upper atmosphere from Cassini Ion Neutral Mass Spectrometer measurements, *Icarus*, *200*, 581–615.
Esposito, L. W., et al. (2004), The Cassini ultraviolet imaging spectrograph investigation, *Space Sci. Rev.*, *115*, 299–361.
Fletcher, L. N., et al. (2015), Seasonal evolution of Saturn's polar temperatures and composition, *Icarus*, *250*, 131–153.
Fray, N., and B. Schmitt (2009), Sublimation of ices of astrophysical interest: A bibliographic review, *Plan. Space Sci.*, *57*, 2053–2080.
Friedson, A. J., A-S. Wong, and Y. L. Yung (2002), Models for polar haze formation in Jupiter's stratosphere, *Icarus*, *158*, 389–400.
Guerlet, S., T. Fouchet, B. Bézard, A. A. Simon-Miller, and F. M. Flasar (2009), Vertical and meridional distribution of ethane, acetylene and propane in Saturn's stratosphere from CIRS/Cassini limb observations, *Icarus*, *203*, 214–232.
Guerlet, S., T. Fouchet, S. Vinatier, A. A. Simon, E. Dartois, and A. Spiga (2015), Stratospheric benzene and hydrocarbon aerosols detected in Saturn's auroral regions, *Astron. Astrophys.*, *580*, A89, doi:10.1051/0004-6361/201424745.
Kim, S. J., J. Caldwell, A. R. Rivolo, R. Wagener, and G. S. Orton (1985), Infrared polar brightening on Jupiter. III. Spectrometry from the Voyager 1 IRIS experiment, *Icarus*, *64*, 233–248.
Kim, S. J., et al. (2012), The three-micron spectral feature of the Saturnian haze: Implications for the haze composition and formation process, *Plan. Space Sci.*, *65*, 122–129.
Kim, Y. H., J. L. Fox, J. H. Black, and J. I. Moses (2014), Hydrocarbon ions in the lower ionosphere of Saturn, *J. Geophys. Res.*, *119*, 384–395.
Koskinen, T. T., et al. (2011), The mesosphere and thermosphere of Titan revealed by Cassini/UVIS stellar occultations, *Icarus*, *216*, 507–534.
Koskinen, T. T., et al. (2013), The density and temperature structure near the exobase of Saturn from Cassini UVIS solar occultations, *Icarus*, *226*, 1318–1330.
Koskinen, T. T., et al. (2015), Saturn's variable thermosphere from Cassini/UVIS occultations, *Icarus*, *260*, 174–189.
Liang, M-C., Y. L. Yung, and D. E. Shemansky (2007), Photolytically generated aerosols in the mesosphere and thermosphere of Titan, *Astrophys. J. Lett.*, *661*, L199–L202.
Moses, J. I., and T. K. Greathouse (2005), Latitudinal and seasonal models of stratospheric photochemistry on Saturn: Comparison with infrared data from IRTF/TEXES, *J. Geophys. Res.*, *110*, E09007, doi:10.1029/2005JE002450.
Moses, J. I., et al. (2015), Evolution of stratospheric chemistry in the Saturn storm beacon region, *Icarus*, *261*, 149–168.
Müller-Wodarg, I. C. F., L. Moore, M. Galand, S. Miller, and M. Mendillo (2012), Magnetosphere-atmosphere coupling at Saturn: 1. Response of thermosphere and ionosphere to steady state polar forcing, *Icarus*, *221*, 481–494.
Press, W. H., S. A. Teutolsky, W. T. Vetterling, and B. P. Flannery (1992), *Numerical Recipes in FORTRAN: The Art of Scientific Computing*, Cambridge Univ. Press, Cambridge, U. K.
Shemansky, D. E., and X. Liu (2012), Saturn upper atmospheric structure from Cassini EUV and FUV occultations, *Can. J. Phys.*, *90*, 817–831.
Sylvestre, M., et al. (2015), Seasonal changes in Saturn's stratosphere inferred from Cassini/CIRS limb observations, *Icarus*, *258*, 224–238.
Vuitton, V., R. V. Yelle, and J. Cui (2008), Formation and distribution of benzene on Titan, *J. Geophys. Res.*, *113*, E05007, doi:10.1029/2007JE002997.
Wong, A-S., A. Y. T. Lee, Y. L. Yung, and J. M. Ajello (2000), Jupiter: Aerosol chemistry in the polar atmosphere, *Astrophys. J. Lett.*, *534*, L215–L217.
Wong, A-S., Y. L. Yung, and A. J. Friedson (2003), Benzene and haze formation in the polar atmosphere of Jupiter, *Geophys. Res. Lett.*, *30*, 1447, doi:10.1029/2002GL016661.